Stifling of Crevice Corrosion and Repassivation: Cathode Area Versus Controlled Potential Decreases Assessed with a Coupled Multi-Electrode Array

Florent Bocher[‡,*,**] *and John R. Scully*[**]

ABSTRACT

The effects of limited remote cathode area on crevice corrosion propagation, repassivation, and anode site reorganization were investigated on AISI 316 stainless steel (UNS S31600) in 0.6 M NaCl at 50°C. Both multiple crevice assemblies and rescaled coupled multi-electrode arrays were utilized. Potentiostatically activated crevices were subjected to conditions that limited propagation by either: (i) stepping the potential downward below the repassivation potential, (ii) performing a downward scan of the potential from high potential, or (iii) decreasing the area of a galvanically coupled platinum cathode situated outside the crevice. In the first two cases, repassivation occurred when the potential reached the lower statistical limit of the repassivation potential measured on creviced specimens in a downward scan. During the galvanically coupled test, repassivation occurred when the galvanic cathodic current supplied became lower than the current required to maintain a couple potential equal to the repassivation potential at the mouth of the crevice. The remaining crevice anode sites first reorganized into smaller active areas deeper in the crevice. Application of Galvele's product for crevice stabilization suggested that such negative potentials lowered the chemical stability product $i \cdot a$ or $i \cdot (a+d)$ below a critical level, with d being the crevice depth and a being the depth of crevice corrosion at individual crevice sites.

KEY WORDS: crevice corrosion, repassivation, stainless steel

INTRODUCTION

One of the earliest stages of crevice corrosion initiation requires the separation of the anode and the cathode, as described by Oldfield and Sutton.[1] This occurs after the oxygen present in the crevice is completely depleted by the local cathodic reactions where the rate of cathodic reactions exceeds the transport rate of oxygen into crevices. The majority of the supporting cathodic reactions are then repositioned into the oxygen-rich environment outside of the crevice and will support the anodic reactions in the crevice. In the case of active/passive metals, these anodic reactions inside the crevice also reach a higher rate once a significant IR drop and highly aggressive solution are achieved in the crevice.[2-3]

The crevice corrosion of active/passive materials is similar to galvanic corrosion because it is driven by a potential difference between the occluded active anode and the bare external passive material serving as the dominant cathode. Unlike galvanic corrosion, the difference of potential does not occur between two different materials, but on the same material where anode/cathode separation and chemistry change have occurred. The area exposed to the bulk solution is the site of the cathodic reaction and portions of the creviced area exposed to the aggressive environment (low pH, high chloride content) are the sites of high-rate anodic reactions. Crevice corrosion is often controlled by the cathodic current availability.[4] It has been shown that the average mass loss of a creviced, stainless steel specimen was linearly correlated to the cathode area.[5]

In the case of crevice corrosion by the dissolution-hydrolysis local acidification mechanism,[6] the stability

Submitted for publication: September 13, 2013. Revised and accepted: June 15, 2015. Preprint available online: June 15, 2015, http://dx.doi.org/10.5006/1120.

‡ Corresponding author. E-mail: fbocher@swri.org.
* Southwest Research Institute, 6220 Culebra Road, San Antonio, TX 78238-5166.
** Center for Electrochemical Science and Engineering, University of Virginia, Charlottesville, VA 22094.

ISSN 0010-9312 (print), 1938-159X (online)

of crevice corrosion also requires that the anodic dissolution occurs at a high enough rate to offset the outward diffusion, and dilution, of the critical aggressive solution present in the crevice so that a low pH, high chloride content solution is maintained at the active crevice site.[6] Consequently, the finite cathode must provide a high enough current or be of large enough area with a uniform enough cathodic reaction rate, or both, to support fast dissolution. In fact, this requirement can be specified in greater detail: the stability product $i \cdot a$ that was developed by Galvele for pitting corrosion provides a relationship between the minimum anodic current density i needed to stabilize a pit of depth a.[7-8] The Galvele's stability product can be modified to provide a simplified approach for crevice corrosion using $i \cdot (a + d)$, with a, the depth of attack, and d, the distance between the crevice mouth and the location of attack.[9] It is possible that both the Galvele stability product $(i \cdot (a + d))$[6] and Pickering critical IR* criteria[3,10] apply and are necessary criteria for crevice corrosion. It is interesting to note that both models might be consistent with crevice corrosion at a critical depth where both criteria are satisfied. On the other hand, it has been shown that the correct E-log(i) behavior of American Iron and Steel Institute (AISI) 316 stainless steel (UNS S31600)[(1)] in a critical crevice solution with Cl^- does not contain an active/passive transition. This suggests that the IR* criterion does not apply, while the Galvale stability product must still be satisfied. This may occur at the mouth if i decreases with depth at a greater rate than $(a + d)$ increases.

The minimum cathodic current needed for crevice corrosion to exist can be related to the updated Galvele's product. The cathodic current available to support the anodic reactions is limited by the surface area of the available immersed uncreviced surface, the kinetic and mass transport processes controlling the rate per unit area, and the distance and solution resistivity between the cathodic reaction area and the crevice, which govern the current distribution over the cathode area.

Many crevice corrosion tests have been conducted with finite anode and cathode areas but these are usually not electrically separated and instrumented so that the cathode current and time-dependent behavior can be investigated. Other crevice tests have been conducted under potentiostatic conditions where the cathode surface area is essentially "infinite" because the potentiostat can supply large cathodic currents to hold a constant potential at the crevice mouth. However, most real crevice exposures involve a finite cathode of limited exposed area, experience a current distribution over a cathode area, or have limited cathode area governed by the wetted surface area.[11] The size of the immersed uncreviced surface can be restricted when the system is either within a limited volume of electrolyte (such as a droplet in atmospheric exposure) or when the solution is only present as a thin film covering the surface with a restricted electrolyte path and a high IR drop that limits the cathodic current to areas proximate to the crevice.[11] Cui, Kelly, and Chen have modeled the maximum cathode current deliverable within a thin film assuming both linear and circular cathode.[4] The cathodic current available was found to linearly increase with the area density of salts in the film because of the role of dissolved salts in lowering the solution resistivity and associated IR drop. Similarly, Agarwal has shown that nonconducting particulates deposited outside the crevice will also affect the amount of cathodic current available by reducing the amount of surface area available and by increasing the IR drop between the cathode site and the crevice mouth via a blocking effect.[12-13]

Multiple types of experimental setup have been used to identify whether there is cathodic control of crevice corrosion. Ellis and LaQue measured the mass loss of a creviced stainless steel specimen with a varying anode and cathode area.[5] Other studies have presented separated anode and cathode galvanically coupled through a zero impedance ammeter.[14-16] The anode was usually formed under a crevice and in the same solution as the distant cathode. Kain[14] and Lee[15] also used two cells connected through a salt bridge. One of the cells, the cathode, contained a test sample in aerated bulk solution; the other cell, the anode, contained an uncreviced test sample in an aggressive solution simulating the concentrated acidified solution of an active crevice. Those testing arrangements offered the possibility of controlling the cathode area, as well as other variables such as the temperature and pH of the solutions. Lee found that the crevice corrosion (galvanic couple) current increases with the cathode-to-anode area ratio for AISI 304 stainless steel (UNS S30400).[15] It has also been shown for both stainless steels and Ni-based alloy (UNS N08825) that the probability of crevice corrosion initiation increases with the cathode-to-anode area ratio.[17]

The objective of this study was to examine the role of a physically limited cathode area coupled to a creviced specimen, on crevice corrosion stifling. Furthermore, the findings were compared to potential hold, potential downward step, and potential scan under instrumented conditions where the cathode and anode behavior could be separately analyzed. Moreover, the coupled multi-electrode arrays (CMEA) method was used to examine with spatial resolution the anode area, the local Galvele criterion, and how particular anode crevice sites reorganized in response to cathode limitations.[18-19] In this study, a platinum cathode was used to avoid strong alloy oxide effects on cathodic reactions.

EXPERIMENTAL PROCEDURES

All experiments were performed in open air using 0.6 mol/L NaCl solution at 50°C. The cell was heated by

[(1)] UNS numbers are listed in *Metals and Alloys in the Unified Numbering System*, published by the Society of Automotive Engineers (SAE International) and cosponsored by ASTM International.

TABLE 1
AISI 316 Stainless Steel Composition (wt%) and PREN[(A)]

	C	Cr	Cu	Fe	Mn	Mo	Ni	P	Si	S	N	PREN
316	0.015	17.32	0.21	Bal.	1.1	2.16	12.11	0.033	0.39	0.002	0.0313	24.95

[(A)] PREN = wt%Cr + 3.3 wt%Mo + 16 wt%N

immersion in a heating bath. The solution was made using reagent grade NaCl and 18.2 MΩ·cm deionized water. The reference electrode was a remotely positioned saturated calomel electrode (SCE) at 25°C, while the counter electrode was a Pt-coated niobium mesh.

The composition of AISI 316, as well as its pitting resistance equivalent number, are shown in Table 1. Plates were used to manufacture lollipop-shaped specimens for the multiple crevice assemblies (MCA) test, while wires were used to assemble the CMEAs.

By combining CMEA with crevice scaling laws derived from experimental data, it is possible to produce highly instrumented crevices with spatially resolved anode sites. Those rescaled crevices enable spatial resolution of the local electrochemistry of corrosion processes as discussed elsewhere.[9,18,20]

The array simulated a planar electrode, with 100 flush-mounted close-packed electrodes (250 μm diameter) electrically coupled through in-line zero resistance ammeters. The electrodes were insulated from each other by a polyimide coating to avoid any unintended short circuits. The polyimide coating also minimized crevice corrosion between the assembly epoxy and the electrode so that attack only initiated on flush-mounted polished faces. The diameter of the electrodes (250 μm) was chosen so that x_{crit} (distance between the crevice mouth and the crevice corrosion initiation site) and the expected zone of crevice corrosion (both predicted from the scaling law factoring in depth and gap) would be larger than the radius of a single electrode. The creviced array and the test assembly are shown in Figure 1. The distance from the crevice mouth always refers to the center of the electrode. Therefore, the first electrode in the crevice will be noted to be 125 μm from the crevice mouth, and the second electrode will be at 375 μm (the diameter plus the radius). Other details of the array setup are presented elsewhere.[18,21-22]

The CMEAs, MCAs, and crevice formers were all ground and polished using SiC paper up to a 1200 grit finish. The Delrin[†] (polyoxymethylene) crevice former was designed to cover approximately 12 columns of five electrodes (totaling 60 electrodes) in the case of AISI 316, leaving eight columns of electrodes exposed outside the crevice former. A torque of 25 in·lbf (3 N·m) over approximately 3 cm^2 was used for all experiments.

A 25-wire-wide spaced AISI 316 CMEA was designed to perform high throughput experiments to determine the crevice initiation and repassivation potential. The crevice initiation and repassivation potentials were identified when the current density was higher and lower than the passive current arbitrarily chosen at $i_{pass} = 10^{-4}$ A/cm^2. All of the cathode electrodes were positioned in a circular fashion equidistant from the crevice mouth so that the initiation and repassivation potentials were independent of position. The potential was swept from –0.1 V_{OCP} to 1 V_{SCE} and back to –0.1 V_{OCP} at a scan rate of 0.1667 mV/s. Anodic potentiodynamic experiments were also performed on a 100-electrode close-packed array. The potential was swept from –0.1 V_{OCP} to 0.7 V_{SCE} at a scan rate of 0.1 mV/s. The potential was held at 0.7 V_{SCE} for 1 h and then swept back to –0.1 V_{OCP} at the same rate.

Crevice corrosion tests were also performed on close-packed AISI 316 CMEA by stepping the potential to higher levels every 24 h in order to allow for the creation of an aggressive critical crevice solution. The uncovered parts of the array were kept at –25 mV_{SCE}, a potential within the passive range, in order to avoid extensive pitting corrosion outside the crevice. The starting scan potential was –25 mV_{SCE} and the creviced array potential was increased by 25 mV increments every 24 h (equivalent to 3×10^{-4} mV/s). The experiments were terminated at 25 mV_{SCE}; this value was chosen during the experiment according to the extent of crevice corrosion observed.

In the final approach, the repassivation and stifling behavior of crevice corrosion of AISI 316 MCA was also studied by potentiostatically applying various potentials where stifling and repassivation might occur. Crevice corrosion was initiated at 0.4 V_{SCE} during 2 h; the potential was then dropped to either 0, –0.1, or –0.2 V_{SCE}.

The setup for natural crevice corrosion with galvanically coupled finite cathodes had eight planar Pt electrodes of various areas connected through switches in series. Pt electrodes were galvanically coupled to the working electrode via zero resistance ammeters through the multichannel microelectrode analyzer (MMA) used to perform the experiments with the CMEA electrode. The total Pt electrode area could be varied from 0.01 cm^2 to approximately 60 cm^2.

The repassivation and stifling behavior of galvanically controlled crevice corrosion of AISI 316 MCA was studied after a potentiostatically forced initiation conducted for 1 h at 0.2 V_{SCE}, which was well above the crevice corrosion initiation potential. The MCA was then galvanically coupled to the variable area Pt cathodes at open circuit potential (OCP). The area of the Pt cathode was decreased every 15 min. Similar tests were

[†] Trade name.

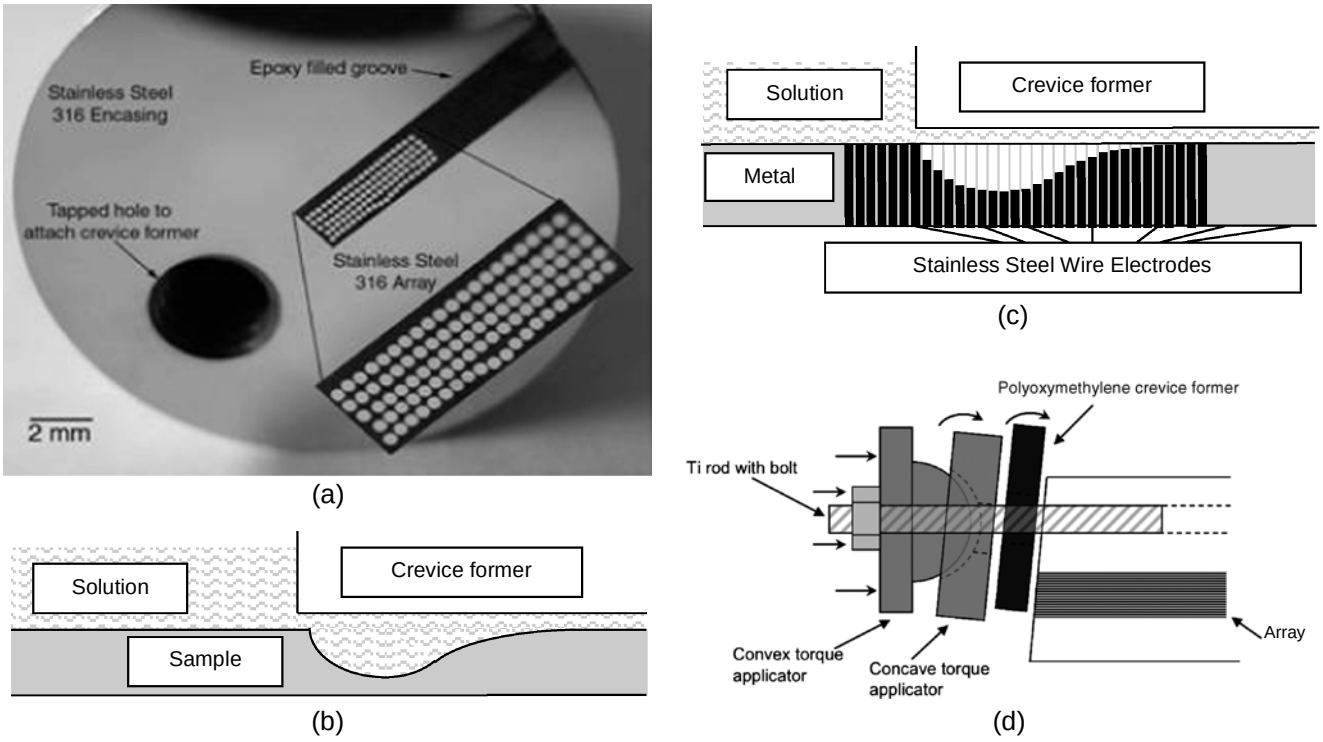

FIGURE 1. *(a) Close-packed array of 100 AISI 316 stainless steel electrodes (250 μm diameter) in a 5×20 arrangement mounted in AISI 316 stainless steel rod. (b) Schematic representation of crevice corrosion attack of a planar sample. (c) Schematic representation of a multi-electrode array. (d) Schematic representation of the crevice former device.*

performed on AISI 316 CMEA. Crevice corrosion was initiated at 0.4 V_{SCE} during 2 h. The CMEA was then coupled to the Pt electrodes at OCP. The area of the cathode was decreased approximately every 30 min. Galvanic crevice corrosion repassivation of AISI 316 CMEA was also performed using greater than 2 d long repassivation steps.

RESULTS

Cumulative Probability of Achieving a Given Crevice Corrosion Potential on Single Electrodes During Upward Potentiodynamic Scans

Figure 2 shows the cumulative probability of the crevice initiation and repassivation potential ranges from far-spaced single AISI 316 stainless steel electrodes in 0.6 M NaCl solution at 50°C. The crevice initiation potential ranged from 0.3 V_{SCE} to 0.8 V_{SCE}, while the repassivation potential was as low as –0.15 V_{SCE}. The OCP of AISI 316 in 0.6 M NaCl and in 5 M HCl at 50°C, as well as the OCP of Pt in aerated 0.6 M NaCl solution at 50°C, are also presented as shaded regions for reference.

The comparison of the OCP of AISI 316 and Pt to the crevice corrosion initiation potential in 0.6 M NaCl shows that the galvanic potential of the AISI 316/Pt couple will always be below the crevice initiation potential. Therefore, crevice corrosion of AISI 316 cannot initiate when coupled to Pt regardless of the area of the Pt electrode.

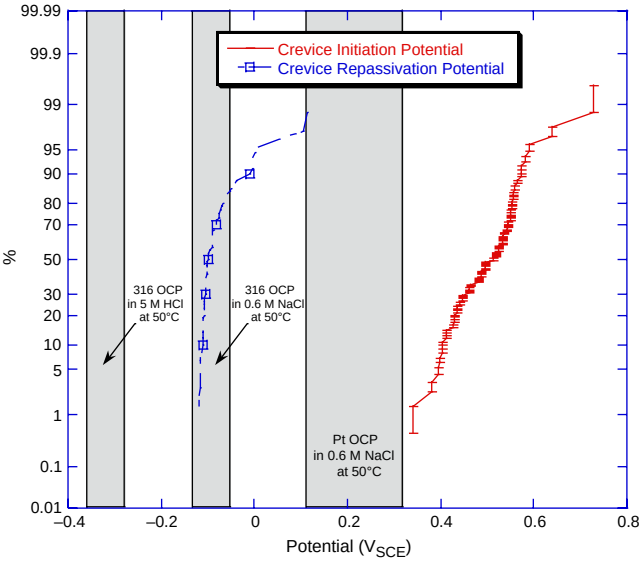

FIGURE 2. *Cumulative probability curve of the distribution of crevice corrosion initiation and repassivation potentials for AISI 316 in 0.6 M NaCl at 50°C. The OCP ranges of AISI 316 in 5 M HCl solution and 0.6 M NaCl solution, as well as Pt in open air 0.6 M NaCl, at 50°C are indicated.*

Five M HCl was chosen as a conservative approximation of what the aggressive solution may be when crevice corrosion is stable. It can be predicted that stable crevice corrosion may be sustained when the

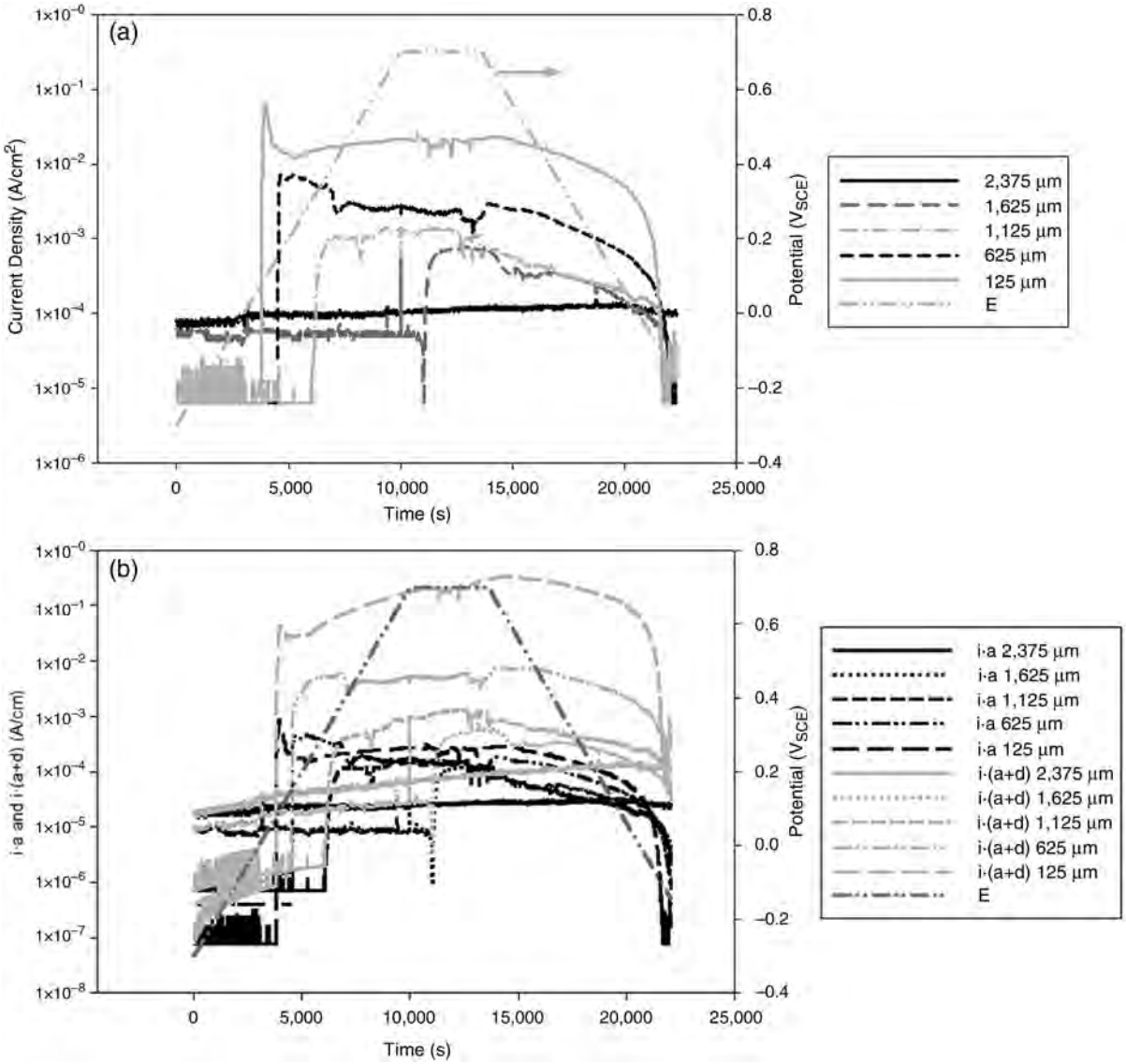

FIGURE 3. *Evolution of (a) current density on individual CMEA electrodes on the first row, and (b) stability product of $i \cdot a$ and $i \cdot (a+d)$ assuming one-dimensional transport and applied potential with time as a function the distance from the crevice mouth during anodic polarization of AISI 316 CMEA under a polyoxymethylene crevice former in 0.6 M NaCl solution at 50°C.*

anodic AISI 316 is coupled to a large enough cathodic Pt electrode, because the value of the crevice corrosion repassivation potential is between the OCP of AISI 316 in 5 M HCl and the OCP of Pt in 0.6 M NaCl. It can also be predicted that stable crevice corrosion will stifle as the galvanic potential decreases, when the area of the Pt electrode is reduced.

Coupled Multi-Electrode Arrays Crevice Behavior During Potential Controlled Experiments

Potentiodynamic Cyclic Measurement — The evolution of the current density as a function of potential and distance from the crevice mouth was measured during potentiodynamic scans on an AISI 316 close-packed CMEA in 0.6 M NaCl solution at 50°C. The results are shown in Figure 3(a). The last line in the legend represents the value of the controlled potential as a function of time. Each other line represents the evolution with time of the average of five measured current density values from five different electrodes. The five electrodes were at the same distance from the crevice mouth (see the representation of the array in Figure 1). The distance was measured from the crevice mouth (situated between two columns of electrodes) to the middle of the column of wires (parallel to the crevice mouth).

After initiation of crevice corrosion, the current density increased rapidly, followed by a plateau in current versus time behavior. The maximum current densities at this plateau decreased with the distance into the crevice from the peak crevice current near the mouth.

Two values of the localized corrosion stabilization product were used for analysis, $i \cdot a$, which had been defined as a pit growth stability indicator by Galvele,[6] and $i \cdot (a+d)$, which was modified based on the original product. The latter was used in order to include both the distance from the crevice mouth, a, and the depth of attack, d, as well as the current density, i, measured on each electrode. Assuming that the depth of attack was homogeneous over the whole surface of a single 250 μm diameter electrode and that local cathodic currents in the crevice are small enough to be neglected, the depth of attack, d, at a time, t_1, can be derived for any electrode in the array using Equation (1), with EW being the equivalent weight, F the Faraday constant, ρ the density, r the radius of the electrode, I(t) the current at a time t, and t_0 the initiation time.

$$d(t_1) = \frac{EW_{316}}{F\rho_{316}\pi r^2}\int_{t=t_0}^{t=t_1} I(t)dt \qquad (1)$$

The evolution of pitting and crevice corrosion stabilization products,[6] $i \cdot a$ and $i \cdot (a+d)$, respectively, with time at various distances from the crevice mouth were determined assuming one-dimensional transport, which was reasonable given that x_{crit} (the distance between the crevice mouth and the crevice corrosion initiation site) is much lower than the crevice width (a being the distance between a given electrode in the MMA under the crevice and the crevice mouth and d the depth of attack).[(2)]

The stability product $i \cdot a$ changes with time. A rapid increase is seen at crevice corrosion initiation, as shown in Figure 3(b). The current density maps reporting spatial distribution of array currents as a function of the potential are shown in Figure 4. The maps are a qualitative representation of the current of each electrode (represented by a shaded gray square) as a function of the position. The rectangle outlined in black indicates the location of the crevice former (not to scale) and the vertical bold black line across the array shows the approximate location of the crevice mouth. The gray scale intensity is linearly related to the current density value. Black squares indicate current densities at or above the maximum displayable current density of 200 $\mu A/cm^2$. The maximum value was chosen to visualize the initiation and repassivation threshold of 10^{-4} A/cm^2. A plus sign indicates anodic current and a minus sign indicates cathodic current.

Crevice corrosion first initiated close to the crevice mouth at approximately 50 mV_{SCE} (see Figure 3) and at a few isolated sites inside and outside the crevice. The attack spread away from the crevice mouth over multiple columns of electrodes as the applied potential was increased. The uncreviced electrodes near the crevice mouth became strongly anodic after crevice corrosion initiated. This is thought to be a result of the outward transport of the aggressive crevice solution resulting in pitting corrosion on the exposed sites. The anodic current density of the electrodes within the crevice decreased with decreasing applied potential. The current density of the anodic sites under the crevice decreased below 10^{-4} A/cm^2 when the applied potential reached 0 V_{SCE}, as seen in Figure 3. Anodic sites with a current density above 200 $\mu A/cm^2$ were still present outside of the crevice, on column 11 (see Figure 4). This may have been a result of the presence of corrosion product outside the crevice mouth. This would form a continuation of the crevice over at least a portion of the first row of electrodes outside of the crevice former, where crevice corrosion would persist at low potential. Alternatively, the crevice former may have covered part of the electrodes in column 11, resulting in crevice corrosion occurring close to the crevice mouth at low potential.

The evolution of crevice corrosion current densities as a function of the distance from the crevice mouth

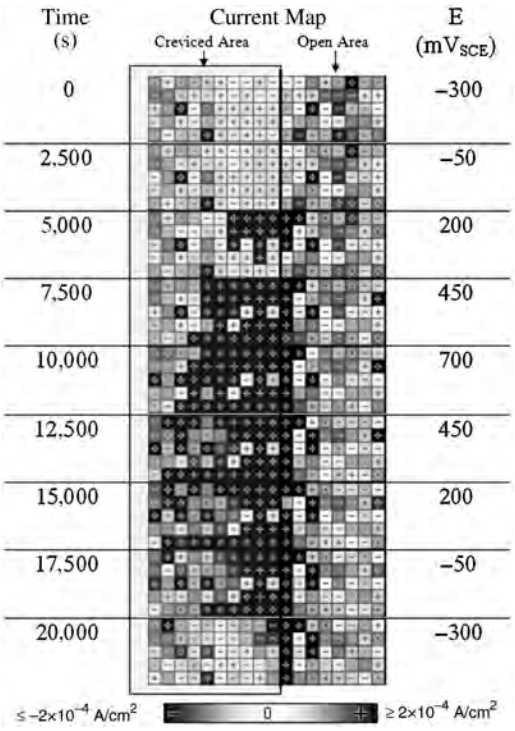

FIGURE 4. *Current density maps of the AISI 316 CMEA showing evolution with time and potential during anodic potentiodynamic scan in 0.6 M NaCl solution at 50°C. Each square represents one electrode (diameter = 250 μm). The black rectangle represents the position of the crevice former (not to scale). The current intensity is indicated by the gray scale and the + or − sign indicates the current sign (+ = anodic). The scale is linear and the display range was chosen to represent the initiation and repassivation thresholds of 10^{-4} A/cm^2.*

[(2)] The use of the $i \cdot (a+d)$ criterion includes the full diffusion distance from the corrosion site to the crevice mouth. This criterion is based on the competition between the creation of metallic ions at the corrosion site and their diffusion to the crevice mouth assuming the need to maintain a nearly saturated crevice solution. It also assumes that the bulk solution concentration is maintained outside the crevice mouth, which is reasonable for stirred conditions. It is assumed that the crevice will be stable and grow when the crevice solution is nearly saturated.

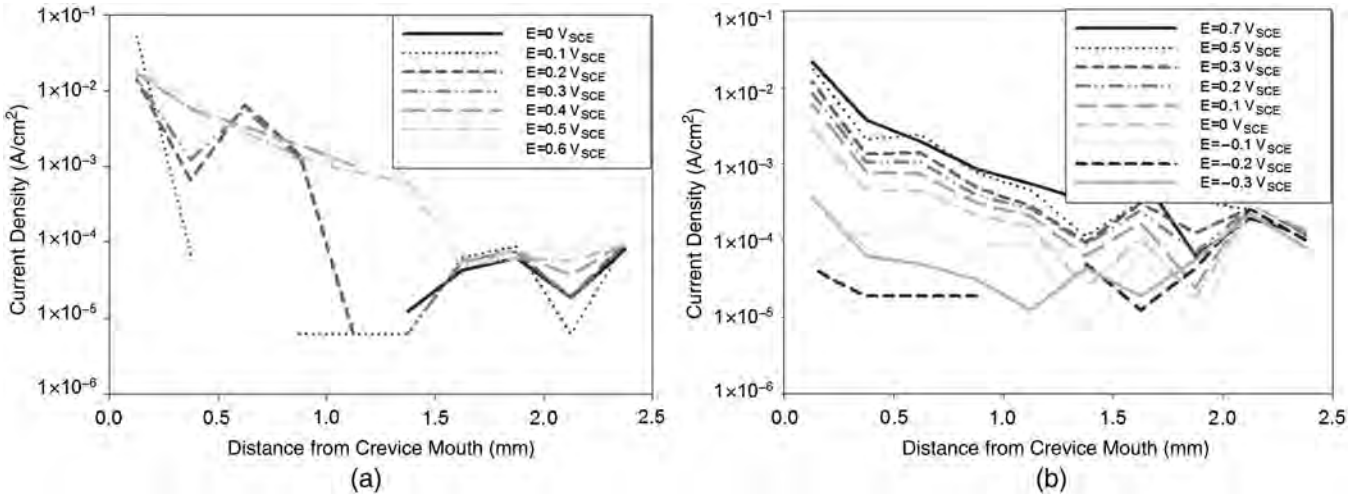

FIGURE 5. *Evolution of the current density as a function of the distance from the crevice mouth and the potential during (a) upward potential sweep and initiation and (b) downward potential sweep and repassivation of crevice corrosion of AISI 316 CMEA in 0.6 M NaCl solution at 50°C.*

within the crevice, at various potentials, during upward and downward scans (0.1667 mV/s), are presented in Figures 5(a) and (b). The plotted data are the average of the data of the five electrodes contained in a column parallel to the mouth, at a fixed given depth. Crevice corrosion initiated first at a critical distance from the crevice mouth on the electrodes between 1.625 mm and 2.375 mm from the crevice mouth at low potentials (0 V_{SCE} and 0.1 V_{SCE}). Crevice corrosion spread closer to the crevice mouth as the potential was increased. The critical distance peak was smaller than the electrode size resolution at potentials over 0.4 V_{SCE}. The highest current densities were measured near the crevice mouth. The current density increased as a function of the distance from the crevice mouth when the potential increased. The current density decreased with decreasing potential. The electrodes further away from the crevice mouth were the first to repassivate. However, a few isolated sites remained activated near the deepest part of the crevice.

Coupled Multi-Electrode Arrays Crevice Behavior During Potential Step Increases and Decreases — Long-term potentiostatic steps experiments were also performed using CMEA and a "quasi-infinite" supporting cathode using the counter electrode. These experiments were aimed at allowing steady state transport conditions to become established, with associated metal ion hydrolysis and acidification to enable crevice corrosion stabilization to take place. The evolution of current density during 24 h at 25 mV_{SCE} at various distances from the crevice mouth is presented in Figure 6. Crevice corrosion initiated again, first on the second electrodes from the crevice mouth, i.e., 375 μm into the crevice, after 2 h. The attack then spread closer to the mouth, as well as deeper into the crevice away from the mouth. Crevice corrosion initiated 625 μm from the crevice mouth after 6 h, and 825 μm from the crevice mouth

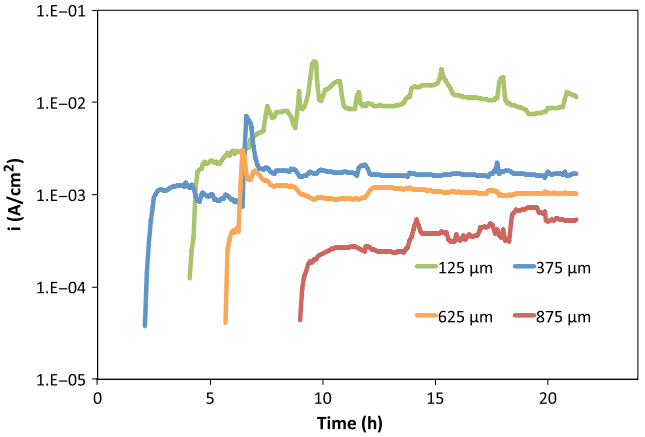

FIGURE 6. *Evolution of the current density with time at various distances from the crevice mouth during crevice corrosion initiation for AISI 316 CMEA at 25 mV_{SCE} in 0.6 M NaCl solution at 50°C with a quasi-infinite cathode (i.e., potentiostat).*

after 9 h. The current densities at each location increased rapidly and then reached a plateau after initiation. Similar behavior was observed during the potentiodynamic test (see Figure 3) in that the plateau current density value was dependent on the distance from the crevice mouth. The localized corrosion stability products as a function of time ($i(t) \cdot a$) are presented in Figure 7. The computed $i(t) \cdot a$ values vs. selected times when the array was potentiostatically held at 25 mV_{SCE} and crevice growth was stable are presented in Figure 8. The pit stability product was fairly stable with time and decreased with the distance from the crevice mouth. The parameter showed no indication of decreasing and repassivation was not seen after 20 h at 25 mV_{SCE}, which is above the repassivation potential seen in Figure 2.

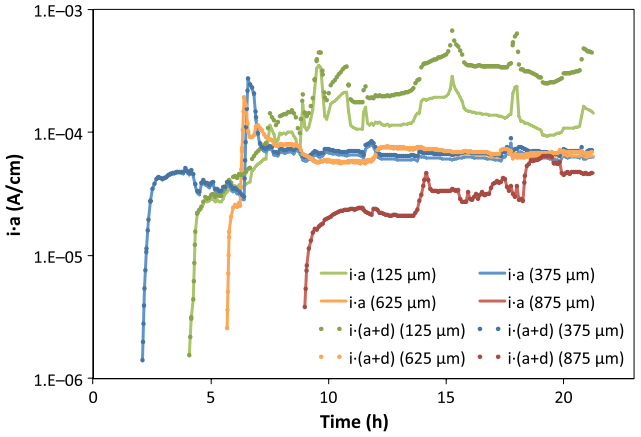

FIGURE 7. *Evolution of $i \cdot a$ and $i \cdot (a+d)$ with time at various distances from the crevice mouth during crevice corrosion initiation for AISI 316 CMEA at 25 mV_{SCE} in 0.6 M NaCl solution at 50°C with a quasi-infinite cathode (i.e., potentiostat).*

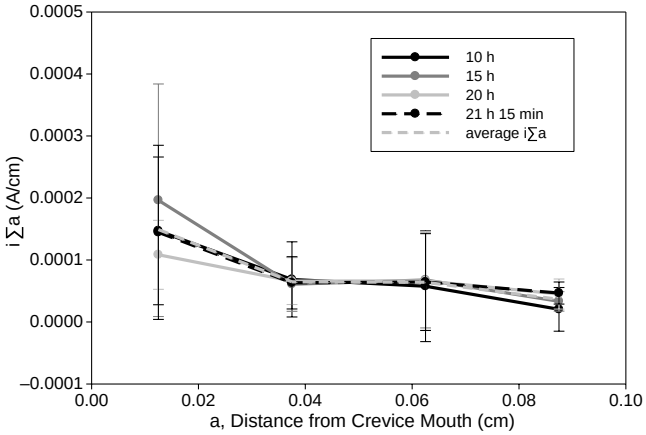

FIGURE 8. *Evolution of $i \cdot a$ and $i \cdot (a+d)$ with distance from the crevice mouth at various times after the current plateau is reached during crevice corrosion initiation for AISI 316 CMEA at 25 mV_{SCE} in 0.6 M NaCl solution at 50°C with a quasi-infinite cathode (i.e., potentiostat).*

Multiple Crevice Assemblies/Coupled Multi-Electrode Arrays High Potential Activation/Low Potential Holds

Stifling and repassivation behavior of conventional AISI 316 multi-crevice assemblies at various potentials after an initiation and growth period for 2 h at 0.4 V_{SCE} are shown Figure 9. The measured current decreased significantly after the potential was stepped down to the indicated potential below the repassivation potential from 0.4 V_{SCE}. Pitting corrosion could be seen on all three specimens. It occurred because crevice corrosion was initiated at 0.4 V_{SCE}. For a lower potential of –0.2 V_{SCE}, the current decayed toward 10^{-5} A indicating repassivation.[3] When the potential was –0.1 V_{SCE}, the current reached approximately 2×10^{-3} A. The current remained constant at 10^{-2} A when the applied potential was 0 V_{SCE}. Thus, repassivation was only seen at –0.2 V_{SCE}, which was near the crevice repassivation potential E_{repass}, as seen in Figure 2. The MCA specimens are shown in Figure 9. The crevice corrosion damage was near the outer edge (mouth of the crevice) as in the case of the CMEA. The crevice corrosion damage was more severe when polarized to 0 V_{SCE}.

[3] The exact active area is unknown.

Galvanically Controlled Crevice Corrosion Behavior when Coupled to Platinum Cathode

Multiple Crevice Assemblies Crevice Corrosion Behavior when Coupled to a Platinum Cathode — Crevice corrosion propagation behavior was followed for a conventional AISI 316 MCA single electrode during coupling to variable area Pt cathodes after potentiostatic initiation at 0.2 V_{SCE}. The evolution of the anodic current as a function of the cathodic area is shown Figure 10(a). The evolution of the coupled potential is shown Figure 10(b) and a post-test micrograph of the MCA is presented Figure 10(c). The galvanic current was larger than the maximum measurement capacity of the potentiostat on the measuring resistor used during the first five steps and 80 min of the test. The galvanic current decreased with cathode area. The decline was first observed when the cathode area was decreased to 1.1 cm^2 because the current was above the maximum current resolution when the cathode area was at or above 10 cm^2. The galvanic current dropped below 10^{-5} A and the crevice repassivated as the Pt cathode area was decreased to 0.11 cm^2 and the couple potential, E_{couple}, became as low as –172 mV_{SCE}. The extent of crevice corrosion after the test is shown in Figure 10(c). Visual inspection of these electrodes confirmed the occurrence of crevice corrosion. However, the severity of attack, in terms of the number of multiple crevice assembly sites attacked and approximate depth of attack, was much lower than in the case of potentiostatic control with a quasi-infinite cathode (Figure 9).

Coupled Multi-Electrode Arrays Crevice Corrosion Behavior when Coupled to a Platinum Cathode — Galvanically controlled repassivation of crevice corrosion was repeated using an AISI 316 CMEA coupled to a variable area Pt cathode. The current density calculations were performed based on the assumption that the anodic current was homogeneous on each individual electrode. This was confirmed by visually observing uniform anodic dissolution of each electrode. The evolution of the anodic current density as a function of time, cathode area, and distance from the crevice mouth is shown in Figure 11(a). Repassivation occurred over approximately a 100 min period, when the cathode area was decreased from 11 cm^2 to 1.1 cm^2. The Galvele pitting/crevice stabilization criterion and the updated $i(t) \cdot (a+d)$ crevice corrosion stability product are shown in Figure 11(b). The pitting and crevice corrosion stability products of all of the active electrodes ranged from

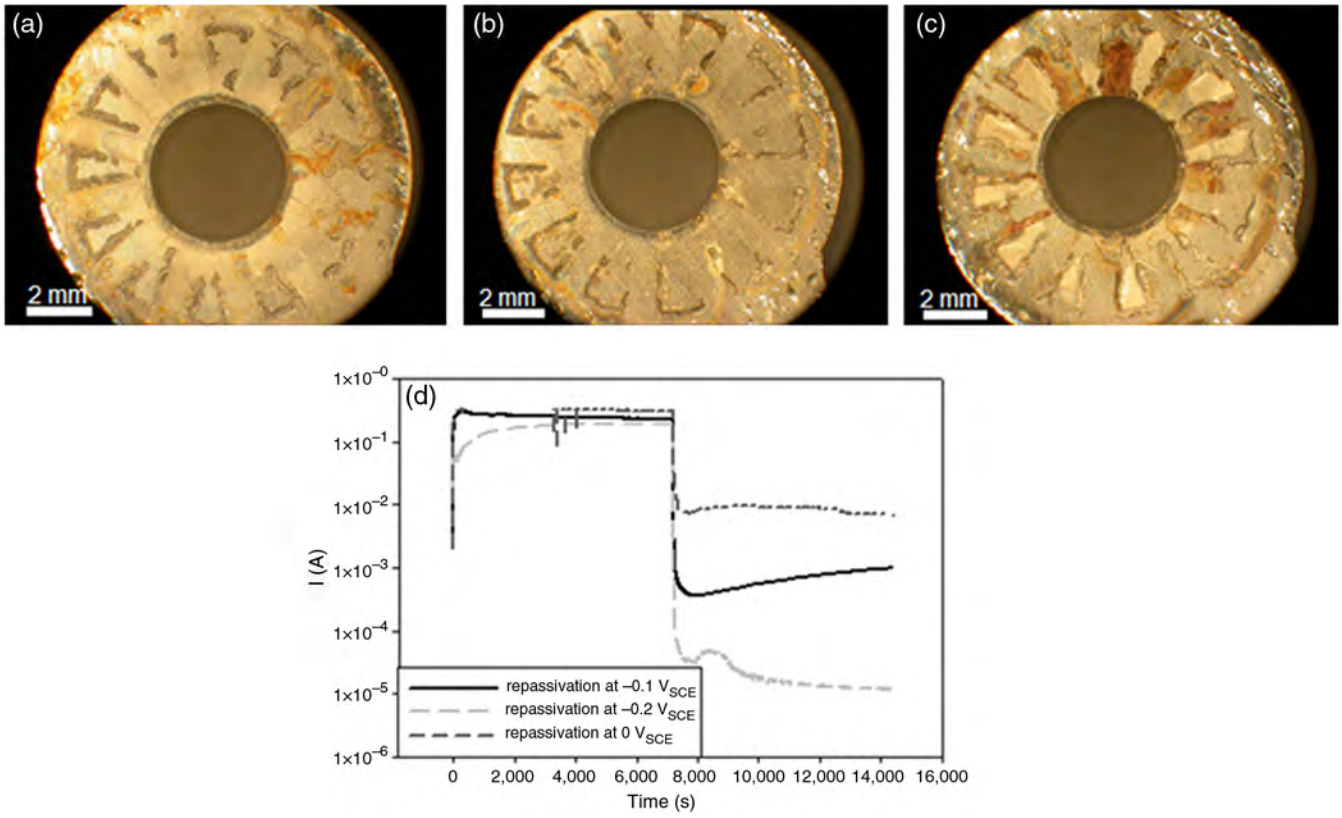

FIGURE 9. *Micrographs of the MCA post-test with repassivation potentials of (a) 0 V_{SCE}, (b) –0.1 V_{SCE}, and (c) –0.2 V_{SCE}. (d) Repassivation of crevice corrosion of AISI 316 MCA after initiation at 0.4 V_{SCE} during 2 h in 0.6 M NaCl solution at 50°C. Repassivation was explored by conducting potential holds for 2 h at –0.2, –0.1 V_{SCE}, and 0 V_{SCE}.*

approximately 2×10^{-3} A/cm to 8×10^{-4} A/cm when the cathode area (A_{cat}) was 11 cm^2 (Figure 11[b]). E_{couple}, taken as the global potential measured with a remote reference electrode, fluctuated and equaled approximately –170 mV_{SCE} at a cathode area of 11 cm^2. Crevice and pitting corrosion repassivated and the localized corrosion stability product plummeted when the cathodic area decreased to 11 cm^2, whereupon E_{couple} decreased to –250 mV_{SCE}.

Moreover, the anodic sites in the crevice also first rearranged before complete repassivation, as the area of the cathode changed, as seen in Figures 12 and 13. The critical distance from the crevice mouth to the most active sites increased as the cathode area decreased. The highest current density value during the first step was found on the second column of electrodes, 375 μm from the crevice mouth. The current density decreased with the distance from the crevice mouth. The current density from the electrode closest to the crevice mouth, 125 μm, decreased drastically with the cathode area. The current density measured 375 μm from the crevice mouth decreased with the cathode area after being constant during the first two steps (until A_{cat} = 51 cm^2). The current densities at 625, 875, and 1,125 μm from the crevice mouth remained individually constant (approximately 1.8 mA/cm^2, 1 mA/cm^2, and ≈0 A/cm^2, respectively) until the cathode area was lowered to 13.6 cm^2 (fifth step). By the fifth step, the highest current density was measured on the electrodes on the third column, 625 μm from the crevice mouth. Once the cathode reached 1.1 cm^2, all actively corroding electrodes had repassivated.

The current density maps present the reorganization of the anodic sites inside the crevice during the repassivation steps (from A_{cat} = 13.6 cm^2 to A_{cat} = 0.1 cm^2), as seen in Figure 13. When the cathode area was switched from 51 cm^2 to 13.6 cm^2, the most active sites inside the crevice with the highest current could already be found on the second column of electrodes (375 μm from the crevice mouth). Three out of the five electrodes on the first column of electrodes were still active after 254 min (125 μm from the crevice mouth). Only one electrode from the first column remained active after 270 min. Four electrodes from the second column, 375 μm from the crevice mouth, remained active when the cathode area was 13.6 cm^2. Only three out of the 14 active electrodes in the four furthest columns from the crevice mouth (distance from crevice mouth = 625 μm to 1,375 μm) repassivated when the cathode area was 13.6 cm^2. A majority of the electrodes outside the crevice were active after 254 min. However, most of those

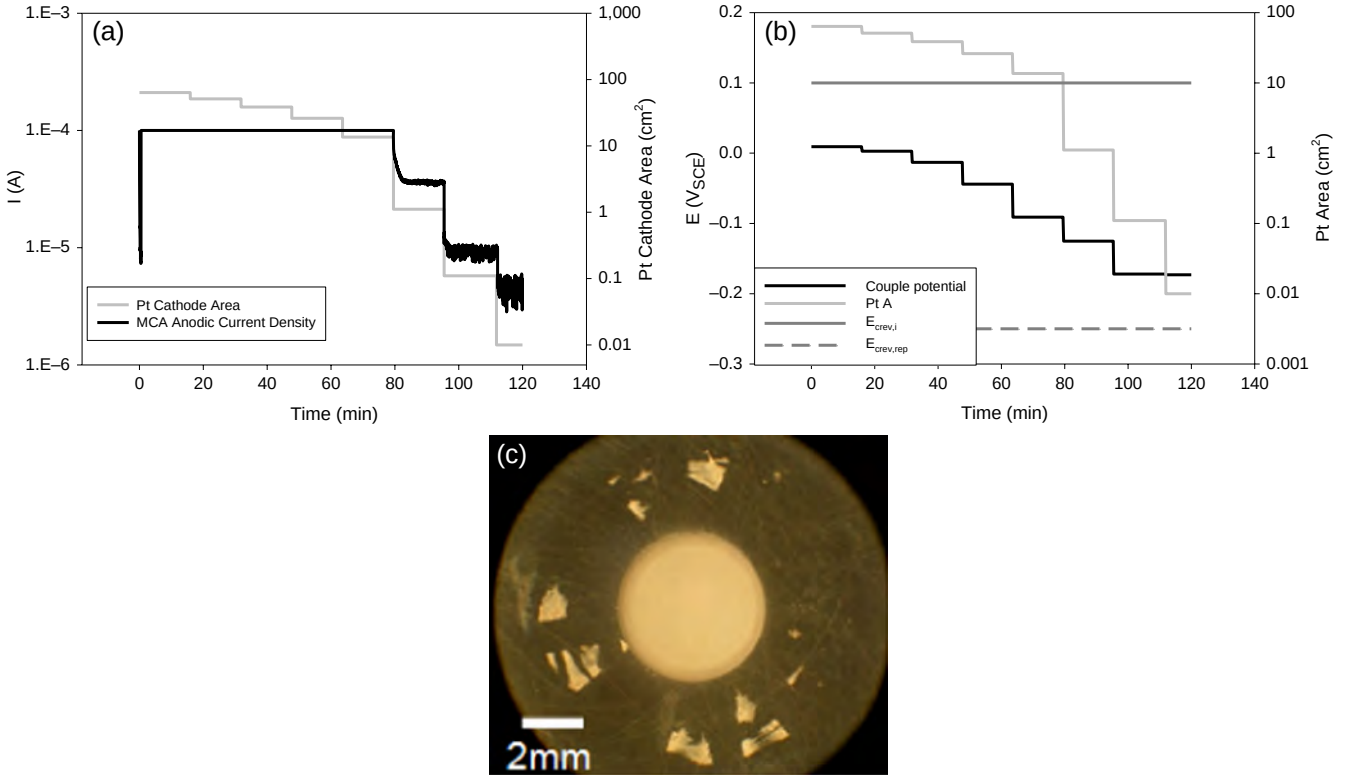

FIGURE 10. *Evolution of (a) the crevice current and (b) the couple potential with time during galvanic repassivation of an AISI 316 MCA coupled to a variable area Pt cathode in 0.6 M NaCl solution at 50°C after crevice corrosion initiation during 1 h at 0.2 V_{SCE}. (c) Micrograph of the AISI 316 MCA after repassivation during galvanic coupling to Pt.*

electrodes repassivated very quickly, with only six remaining active after 279 min. All of the electrodes outside and inside the crevice former repassivated within 10 min after the cathode area was switched to 1.1 cm^2 and subsequently, E_{couple} decreased to –250 mV_{SCE}.

DISCUSSION

Potentiostatic Versus Potentiodynamic Crevice Corrosion Stabilization

Potentiodynamic and potentiostatic experiments were performed using a quasi-infinite source of cathodic current, by using a potentiostat, in order to obtain a baseline for comparison of the galvanically controlled crevice corrosion experiments. Similar current density and spatial organization with time were seen during potentiodynamic and potentiostatic experiments (see Figures 3 and 6). The current map of the potentiodynamic experiments is presented Figure 4. It is interesting to note that the initiation potential measured using the potentiodynamic experiments was not lower than 80 mV_{SCE}, while crevice corrosion initiated during the potentiostatic hold at 25 mV_{SCE} after at least 2 h of exposure. This implies that the equilibrium transport condition was not reached during the potentiodynamic test and required time for chemistry changes that were not available in the finite time such that a potential scan could reach higher potentials. This is not a new result.[23] The crevice gap dimension will also have an impact on the chemistry development, location of crevice corrosion, and the initiation, as well as the repassivation potentials.[24] The resulting change in crevice solution volume will affect the development of the aggressive chemistry required for crevice corrosion initiation and consequently, the IR drop needed to sustain it.[24]

The Crevice Corrosion Stability Product Compared to the Pitting Corrosion Stability Product

The localized corrosion stability products calculated for the potentiostatic crevice corrosion initiation experiment are presented as a function of the distance from the crevice mouth in Figure 7. The stability products do not change significantly with time on each electrode, but a wider range of values was observed closer to the mouth. The absolute value of the stability product was significantly lower than the reported stability product (0.2×10^{-2} A/cm) in the case of metastable pits, possibly because the effective cation and chloride diffusion coefficients were actually lower than the faster values assumed in earlier work.[25-26] This would mean that a lower product of $i \cdot a$ would also correspond to a nearly saturated salt concentration. The

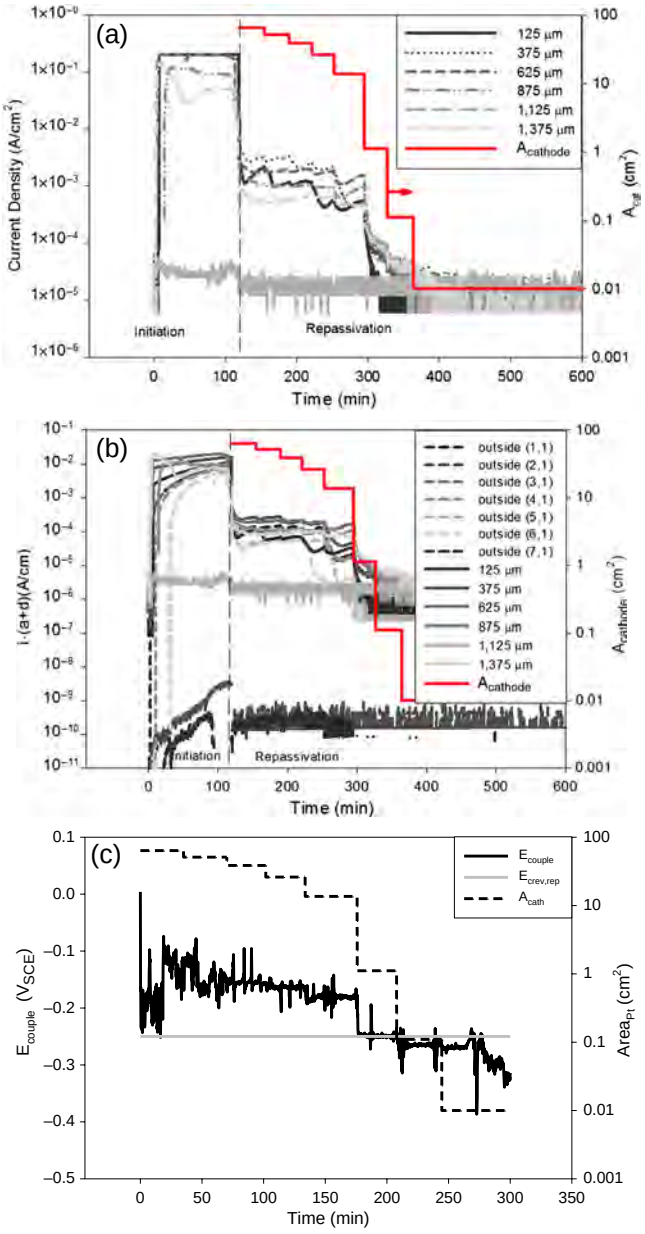

FIGURE 11. *Evolution of (a) the crevice current density and (b) $i \cdot (a+d)$ in the crevice and $i \cdot d$ outside the crevice with time during galvanic repassivation of an AISI 316 CMEA coupled to a variable area Pt cathode in 0.6 M NaCl solution at 50°C after crevice corrosion initiation during 2 h at 0.4 V_{SCE}. Only row 1 is displayed. (c) Evolution of the couple potential with time.*

pit stabilization product value at room temperature is on the order of 0.2×10^{-2} A/cm, assuming a cation diffusivity of 10^{-5} cm^2/s to 10^{-6} cm^2/s.[6] The crevice corrosion stabilization product value may also be lower at 50°C as a result of lower cation diffusivity at higher temperature, as well as extrinsic diffusion limitations inside the crevice resulting from corrosion product buildup, or geometric factors such as a re-entrant or tortuosity in the corrosion site geometry.

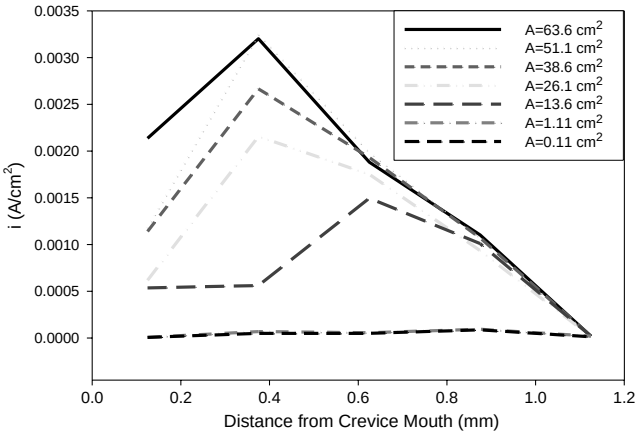

FIGURE 12. *Evolution of the crevice current density as a function of the distance from the crevice mouth and the cathode area during crevice repassivation of AISI 316 CMEA in 0.6 M NaCl solution at 50°C with variable area galvanically coupled Pt cathode. The current density was taken at the end of each step.*

Platinum Cathodes

The cathode area had a weak effect on couple potential for areas much larger than the creviced area in both CMA (Figure 10[c]) and CMEA tests (Figure 11[c]). However, a significant effect was seen on couple potential in both MCA and CMEA tests when the cathode area was below 1 cm^2. The crevice propagation current was strongly dependent on cathode area at the same threshold area of 1 cm^2. Consistent with this observation is the finding that the galvanic current between the Pt cathode and the single electrode MCA decreased with the Pt area and was below 10^{-4} A when the cathode area was less than 10 cm^2 (see Figure 10[a]). However, the potential did not reach the repassivation potential measured previously (see Figure 10[b]). Consequently, it was not possible to determine accurately the effect of the Pt cathode area on repassivation using a single creviced AISI 316 electrode. The CMEA offers better current resolution in order to assess crevice corrosion repassivation on a local scale. The current densities measured using a CMEA were relatively independent of cathode area at large cathode areas but decreased significantly when the area was decreased to 1.1 cm^2, as shown in Figure 11(a). The couple potential dropped slightly below the repassivation potential when the cathode area was 1.1 cm^2 (see Figure 11 [c]). This confirms that when the couple potential reached the repassivation potential measured by the potentiodynamic method, crevice corrosion repassivated. However, the spatial rearrangement of the crevice anode site, observed as the cathode area and the couple potential decreased (see Figure 12), changed as well, which cannot be seen in the MCA measurement. The CMEA crevice behavior during cathode area changes also differed from the potentiodynamic case (see Figure 5). The current densities of all electrodes decreased more or less simultaneously with the potential

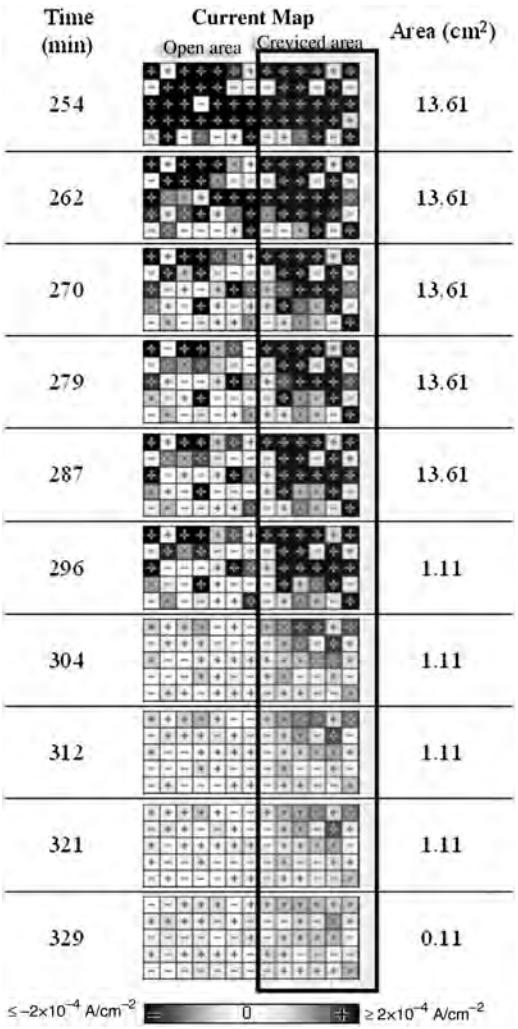

FIGURE 13. *Current density maps of the AISI 316 CMEA evolution with time and Pt cathode area in 0.6 M NaCl solution at 50°C after switching from potentiostatic control to control with a finite cathode. Each square represents one electrode. The shaded gray box represents the position of the crevice former (not to scale). The current intensity is indicated by the gray scale and the + or − sign indicates the current sign (+ = anodic). The scale is linear and the display range was chosen to represent the initiation and repassivation threshold of 10^{-4} A/cm^2.*

during the potentiodynamic scan, and consequently, the most active electrodes remained near the crevice mouth. In contrast, for the CMEA with decreasing Pt area, the highest current densities were found further away from the crevice mouth when the Pt area decreased. This rearrangement of the most active electrodes is clearly seen in Figure 13. This rearrangement was speculated to occur for two reasons. The galvanic current decreased with the cathode area. Either all electrodes could experience a lower current density or some sites could repassivate and the remaining galvanic current could be concentrated on a few remaining electrodes that can maintain an aggressive solution chemistry.[24] Apparently, the anodic reaction rate close to the mouth decreased and the local aggressive solution diffused out. In this situation, it became more difficult to maintain a high value of $i(t) \cdot a$, leading to repassivation of the electrodes closest to the mouth. The anodic dissolution rate can be concentrated and maintained on the electrodes deeper in the crevice because the product of $i(t) \cdot a$ can be maintained at a higher level further away from the mouth despite a greater IR drop. This is in fact seen in Figure 11(b). Importantly, the ohmic voltage does not drop the potential of these deep remaining sites below a level that forces repassivation, because the overall galvanic current between the inside and outside of the crevice is lower and hence, the ohmic voltage drop is lower.

Effect of Cathodic Reaction Kinetics on Crevice Corrosion Behavior

Repassivation potentials are often not meaningful because they are so technique-dependent in the localized corrosion of stainless steels.[27-28] One example of a meaningful potential where repassivation of a crevice can be forced is when the cathode potential at the mouth is forced to the crevice OCP when the coupled cathode area is reduced.[7] Further insight can be developed regarding the potential range between the anode and cathode by comparing the OCP of AISI 316 in 0.6 M NaCl (cathode in the bulk solution) and in 5 M HCl (anode in the crevice aggressive solution) at 50°C, as shown in Figure 2. The OCP of an AISI 316 cathode (assumed to be represented by the OCP in 0.6 M NaCl solution) is higher than the average crevice OCP in an aggressive solution (5 M HCl) that is assumed to be close to the OCP of the anode. When the cathode area is reduced, the remaining cathode is forced to become polarized toward the anode OCP in order to provide high current.

In this study, a Pt cathode was used because it resulted in a galvanic couple that was free of substantial time-based oxide film effects at the cathode. The OCP of the Pt in the bulk solution was 200 mV above the average crevice OCP for AISI 316 (see Figure 2). The experimental coupling of the Pt cathode to the anodic creviced AISI 316 made for a more ideal experimental situation that enabled focus on the anode with a simplified cathode. It also enabled exploration of a larger range of potentials.

As discussed by Cui, et al., a cathode is polarized somewhere between its OCP, at distances far from the crevice mouth, and the potential of the crevice mouth, due to IR drop.[29] The integrated sum of cathodic currents over areas at these potentials must equal the sum of the anode currents. In the simplified arrangement with a separated Pt cathode and a creviced AISI 316 anode, the galvanic couple potential also varies within a range limited by the anode and cathode OCPs. The spatial distribution is less important than the cathode area in this study because the Pt cathode was always close to the crevice mouth (approximately 4 cm), uniformly accessible, and fully immersed in a conductive

solution. However, the couple potential decreased toward the anode OCP as the Pt cathode area was decreased (Figure 11[c]). This is different from the study of crevice corrosion performed with potentiostats during which the current can change independently under constant applied potential if the localized solution composition changes.

The cathodic current as a function of time, potential, and area on the Pt electrode was compared to the theoretically calculated values in order to validate the results described above. The experimental cathodic current was measured by performing potentiostatic holds at –0.25 V_{OCP} and –0.5 V_{OCP} at various areas. The potentials' holds values were chosen based on their relevance to crevice corrosion. The currents at –0.25 V_{OCP} and –0.5 V_{OCP} were plotted as a function of the area, and at various time, from 0.01 s to 1,000 s, on a logarithmic scale (Figures 14 and 15). The potentiostatic currents were compared to the theoretical cathodic currents for the oxygen reduction reaction (ORR). The theoretical cathodic currents were calculated using Equations (2) through (5), where A is the cathode area, η_{ORR} is the cathodic overpotential, b_c is the cathodic Tafel slope for the ORR, F is Faraday's constant, and t is time. It was assumed that n = 4, $D = 8\times10^{-6}$ cm^2/s, and $C_{O2} = 2.5\times10^{-7}$ mol/cm^3.

$$I_{total} = i_{total} \times A_{cat} \quad (2)$$

$$\frac{1}{i_{total}} = \frac{1}{i_{CT}} + \frac{1}{i_{lim}} \quad (3)$$

$$i_{CT} = i_0 \times \exp\left(\frac{-2.3\times\eta_{ORR}}{b_c}\right) \quad (4)$$

$$i_{lim} = \frac{nFAC\sqrt{D}}{\sqrt{(\pi t)}} \quad (5)$$

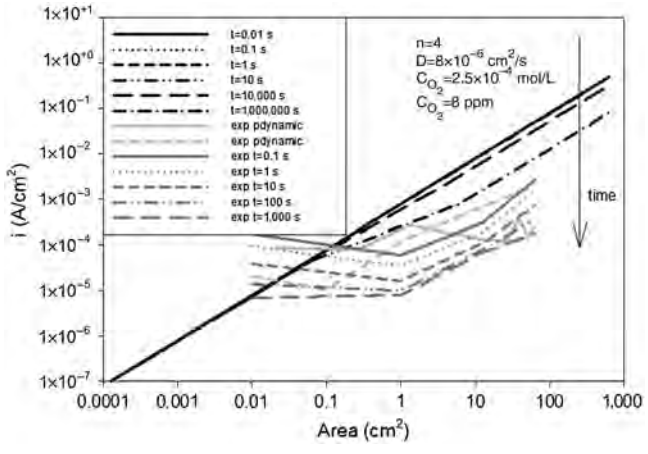

FIGURE 14. *Evolution of the theoretically derived i_{tot} and experimental (exp) i_{tot} (from potentiodynamic scan and from potentiostatic test at –0.25 V_{OCP}) for the ORR reaction on Pt in 0.6 M NaCl solution with the indicated assumed parameters as a function of the Pt cathode area and the time.*

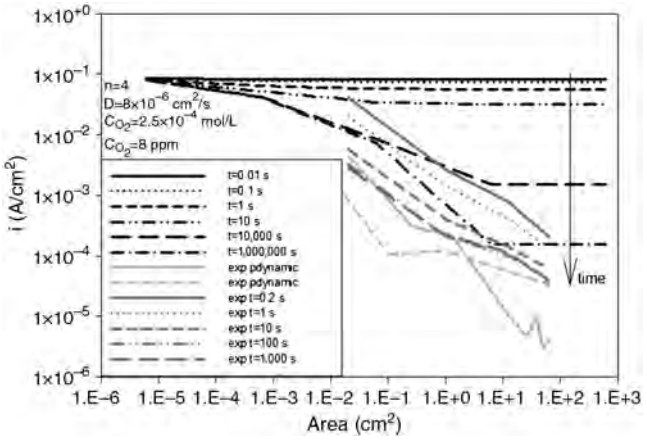

FIGURE 15. *Evolution of the theoretically derived i_{tot} and experimental (exp) i_{tot} (from potentiodynamic scan and from potentiostatic test at –0.5 V_{OCP}) for the ORR reaction on Pt in 0.6 M NaCl solution with the indicated assumed parameters as a function of the Pt cathode area and the time.*

The calculated cathodic current increased with cathode area, at –0.25 V_{OCP}. The cathodic current decreased with time according to Equation (5), independent of the oxygen reduction overpotential, because the diffusion boundary layer grew. The calculated current decreased as a function of time with a steeper slope when the potential was more negative because the cathodic current was under mixed charge transfer and mass transport control at approximately –0.25 V_{OCP}, while it was primarily mass transport controlled at –0.5 V_{OCP}. Experimental results followed the same trends. However, experimentally obtained currents were lower than theoretical values. A possible explanation is that it may be indicative of a poisoned Pt electrode where some ORR sites were blocked. However, the data presented in this article are not sufficient to make this conclusion.

The calculated and measured total cathodic current (for the Pt electrodes) are plotted along with the crevice current measured during the galvanic repassivation of single MCA electrodes (see Figure 16). The repassivation current was also obtained from the galvanic current on Pt at the stainless steel repassivation potential (Figure 16). It is interesting to note that both the experimentally measured crevice current and the measured total cathodic current decreased below the current required to keep the mouth of the crevice above the repassivation potential when the cathode area decreased from 11.1 cm^2 to 1.1 cm^2. This confirmed that it was possible to predict the cathodic area required to maintain crevice corrosion based on the potentiostatic measurement of the Pt cathodic current at the repassivation potential.[4] However, as explained earlier,

[4] This is under conditions of uniform current and potential distribution across the anode surface. The area could differ when current and potential distributions are not uniform.

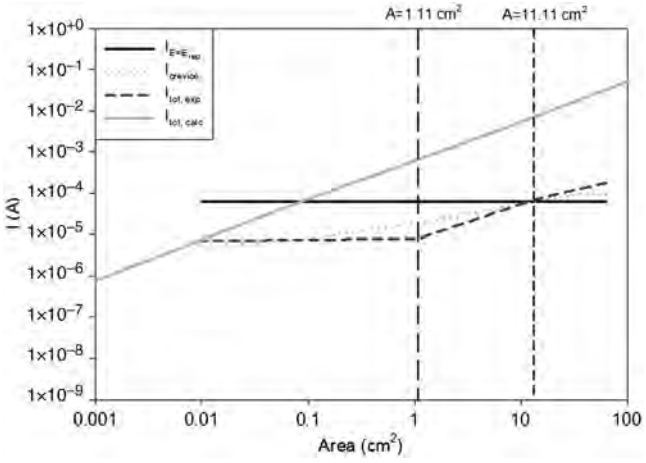

FIGURE 16. *Comparison of the theoretically (calc) derived I_{tot} and measured (exp) I_{tot} total cathodic current for ORR on Pt compared to the measured galvanic crevice current (from the galvanic experiments on the MCA coupled to Pt, at the end of each step). $I_{crevice}$, and the potentiostatic current at the repassivation potential, $I_{E=Erep}$ (of AISI 316 in 5 M HCl solution, as a function of the Pt cathode area).*

because of differences between the theoretical and experimental results, it is not possible to use the theoretical calculation as a basis for comparison.

In summary, three things happen during galvanic crevice corrosion as the cathode area is decreased. These are: (a) reorganization of the anode to a more limited number of anodic sites deeper in the crevice, (b) a decrease in the galvanic couple potential, as well as the galvanic "crevice" couple current, particularly when the cathodic reaction on the external cathode becomes near its mass transport limited region, and (c) chemistry changes and subsequent repassivation of the crevice either when the potential at the crevice mouth reaches the repassivation potential or the OCP of the crevice material. At this point, even reorganization of the crevice anode to smaller areas cannot maintain active crevice corrosion.[24,29]

CONCLUSIONS

❖ The crevice corrosion study presented new insights on the initiation and repassivation of crevice corrosion of AISI 316 stainless steel using a CMEA. CMEAs offered a way to follow the initiation, propagation, and repassivation of crevice corrosion as a function of the location inside the crevice. The area of the anodic sites was found to decrease and reorganize toward sites deeper in the crevice as the cathode size, and therefore the available current, decreases. A Pt cathode in the bulk solution has an OCP higher than that of stainless steel in an aggressive solution. However, the crevice galvanic couple potential between Pt and a stainless steel crevice decreased rapidly when the cathodic reaction on the external Pt cathode approached the mass transport limit for the primary cathodic reaction that supports crevice corrosion. It was found that repassivation occurred when the cathodic current, determined experimentally and theoretically assuming that the oxygen reduction reaction is the operative cathodic reaction, reached the current value where the cathode potential and, in turn, the crevice mouth potential was equal to either the repassivation or OCP of the active anode sites. As the Pt area was decreased, the cathode current and couple potential were found to decrease until the repassivation of the stainless steel creviced sample occurred by this process. Under a variety of situations involving a finite cathode, even reorganization of the crevice anode to smaller areas could not maintain active crevice corrosion.

ACKNOWLEDGMENTS

The support of this work from the Office of Science and Technology and International, Office of Civilian Radioactive Waste Management, U.S. Department of Energy is gratefully acknowledged. The work is performed as part of the DOE Multi-University Corrosion Cooperative under Cooperative Agreement DE-FC28-04RW12252. Additional support was obtained for JRS from ONR MURI titled "Understanding Atomic Scale Structure in Four Dimensions to Design and Control Corrosion Resistant Alloys" on grant number N00014-14-1-0675.

REFERENCES

1. J.W. Oldfield, J.W. Sutton, *Br. Corros. J.* 13 (1978): p. 13-22.
2. B.A. Shaw, P.J. Moran, P.O. Gartland, *Corros. Sci.* 32 (1991): p. 707-719.
3. R.S. Lillard, J.R. Scully, *J. Electrochem. Soc.* 141 (1994): p. 3006-3015.
4. Z.Y. Chen, F. Cui, R.G. Kelly, *ECS Transactions* 3 (2007): p. 443-457.
5. O.B. Ellis, F.L. LaQue, *Corrosion* 7 (1951): p. 362-364.
6. J.R. Galvele, *J. Electrochem. Soc.* 123 (1976): p. 464-474.
7. J. Srinivasan, R.G. Kelly, *Corrosion* 70 (2014): p. 1172-1174.
8. J.R. Galvele, J.B. Lumsden, R.W. Staehle, *J. Electrochem. Soc.* 125 (1978): p. 1204-1208.
9. F. Bocher, F. Presuel-Moreno, J.R. Scully, *J. Electrochem. Soc.* 155 (2008): p. C256-C268.
10. K. Cho, H.W. Pickering, *J. Electrochem. Soc.* 138 (1991): p. L56-L58.
11. M.T. Woldemedhin, M.E. Shedd, R.G. Kelly, *J. Electrochem. Soc.* 161 (2014): p. E3216-E3224.
12. A.S. Agarwal, U. Landau, J.H. Payer, *J. Electrochem. Soc.* 157 (2010): p. C9-C17.
13. A.S. Agarwal, U. Landau, J.H. Payer, *J. Electrochem. Soc.* 155 (2008): p. C269-C278.
14. R.M. Kain, T.S. Lee, "Recent Developments in Test Methods for Investigating Crevice Corrosion," in *Laboratory Corrosion Tests and Standards*, ASTM STP 866, eds. G.S. Haynes, R. Baboian (Philadelphia, PA: ASTM, 1985), p. 299-323.
15. T.S. Lee, "A Method for Quantifying the Initiation and Propagation Stages of Crevice Corrosion," in *Electrochemical Corrosion Testing*, ASTM STP 727, eds. F. Mansfeld, U. Bertocci (Philadelphia, PA: ASTM, 1981), p. 43-68.
16. I.L. Rosenfeld, I.K. Marshakov, *Corrosion* 20 (1964): p. 115t-124t.
17. A.J. Sedriks, *Corrosion of Stainless Steels*, 2nd ed. (Hoboken, NJ: Wiley InterScience, 1996).
18. F. Bocher, F. Presuel-Moreno, N.D. Budiansky, J.R. Scully, *Electrochem. Solid-State Lett.* 10 (2007): p. C16-C20.
19. N.D. Budiansky, F. Bocher, H. Cong, M.F. Hurley, J.R. Scully, *Corrosion* 63 (2007): p. 537-554.

20. J.S. Lee, M.L. Reed, R.G. Kelly, *J. Electrochem. Soc.* 151 (2004): p. B423-B433.
21. F. Bocher, F. Presuel-Moreno, N.D. Budiansky, J.R. Scully, "Coupled Multi-Electrode Investigation of Crevice Corrosion of 316 Stainless Steel and NiCrMo Alloy 625," in Critical Factors in Localized Corrosion 5: A Symposium in Honor of Hugh S. Isaacs, eds. M. Missert, S. Virtanen, A.J. Davenport, M.P. Ryan (Pennington, NJ: ECS, 2006), p. 105.
22. F. Bocher, F. Presuel-Moreno, N.D. Budiansky, J.R. Scully, "Investigation of Crevice Corrosion of AISI 316 Stainless Steel and Ni-Cr-Mo Alloy 625 Using Coupled Multi-Electrode Arrays," CORROSION 2007, paper no. 587 (Houston, TX: NACE International, 2007).
23. N. Sridhar, G.A. Cragnolino, *Corrosion* 49 (1993): p. 885-894.
24. N. Sridhar, D.S. Dunn, *Corrosion* 50 (1994): p. 857-872.
25. D.E. Williams, J. Stewart, P.H. Balkwill, *Corros. Sci.* 36 (1994): p. 1213-1235.
26. G.S. Frankel, L. Stockert, F. Hunkeler, H. Boehni, *Corrosion* 43 (1987): p. 429-436.
27. A. Anderko, N. Sridhar, D.S. Dunn, *Corros. Sci.* 46 (2004): p. 1583-1612.
28. A. Anderko, N. Sridhar, L.T. Yang, S.L. Grise, B.J. Saldanha, M.H. Dorsey, *Corros. Eng. Sci. Technol.* 40 (2005): p. 33-42.
29. F. Cui, F. Presuel-Moreno, R.G. Kelly, *Corros. Sci.* 47 (2005): p. 2987-3005.